

# Modeling Turbulent Flows with LSTM Neural Network

Hugo D. Pasinato<sup>1</sup> and Nicolás F. Moguilner Rhe<sup>2</sup>

<sup>1,2</sup>(Universidad Tec. Nacional, FRP, Argentina)

<sup>1</sup>*hugopasinato@frp.utn.edu.ar*

In this study, we explore the application of an artificial recurrent neural network (RNN) called Long Short-Term Memory (LSTM) as an alternative to a turbulent Reynolds-Averaged Navier-Stokes (RANS) model. The LSTM models are utilized to predict the shear Reynolds stress in developed and developing turbulent channel flows. We conduct comparative analyses, comparing the LSTM results propagated through computational fluid dynamics (CFD) simulations with the outcomes from the  $\kappa - \epsilon$  model and data acquired from direct numerical simulation (DNS). These analyses demonstrate a good performance of the LSTM approach.

## 1 Introduction

Fluid flow predictions are of utmost importance in various fields of engineering, including mechanical, chemical, and aeronautical, to achieve diverse objectives such as design optimization and equipment enhancement. Many of these engineering applications involve turbulent flows, which require the use of Reynolds-averaged Navier-Stokes (RANS) modeling. RANS is a commonly employed technique for high-velocity scenarios with high Reynolds numbers. It involves utilizing the Reynolds averaging method to derive the time-averaged general equations of fluid motion, known as the RANS equations (Pope [2000]). These equations, expressed in dimensionless form using tensor notation, are the conservation of mass

$$\frac{\partial U_i}{\partial x_i} = 0, \quad (1)$$

and the momentum equations

$$\frac{\partial U_i}{\partial t} + \frac{\partial(U_j U_i)}{\partial x_j} = -\frac{\partial P}{\partial x_i} + \frac{1}{Re_\tau} \frac{\partial^2 U_i}{\partial x_j \partial x_j} - \frac{\partial \langle u_j u_i \rangle}{\partial x_j}, \quad (2)$$

where  $U_i$  (equivalent to  $U$ ,  $V$ , and  $W$ ), is the mean velocity and  $P$  the mean pressure,  $x$  and  $t$  are the space and time coordinates, respectively, and  $Re_\tau$  is the friction Reynolds number  $u_\tau \delta / \nu$ . All variables are non-dimensionalized using the friction velocity,  $u_\tau$  and half the distance between walls,  $\delta$ , which represent the characteristic velocity and length scales. Furthermore, when the original Navier-Stokes equations are time-averaged, a tensor arises consisting of new unknowns, known as the Reynolds stress tensor,  $\langle u_j u_i \rangle$ . Given that this tensor is symmetric, for solving these equations there are 6 new unknowns, in addition to  $U_i$  and  $P$ .

Previous task involves incorporating a procedure or method for computing these 6 new unknowns (the velocities  $U$ ,  $V$ , and  $W$  and pressure  $P$  are found using the conservation equations of momentum and mass). These techniques are called RANS modeling for turbulence, as commented above, with the Kappa-Epsilon model being an example of them. In general, these models employ a pseudo viscosity that is determined based on the influence of turbulence. This approach draws an analogy between the behavior of a Newtonian fluid and that of a turbulent flow. By incorporating this pseudo viscosity, the models aim to capture the characteristics and dynamics of turbulent flows in a manner similar to how a Newtonian fluid behaves.

RANS models depend on empirically-determined constants that are calibrated using experimental turbulent flows or more accurate techniques such as Large Eddy Simulation (LES) or Direct Numerical Simulation (DNS). However, when these models are utilized beyond the range of their calibrated constants, their predictions may lack accuracy. This represents the primary challenge associated with RANS techniques.

Following a prolonged period of stagnation, RANS modeling is now entering a new phase with the integration of Artificial Intelligence (AI) techniques. AI involves a diverse range of data-driven algorithms, ranging from well-known methods like linear regression to more advanced concepts like neural networks. With the availability of high-fidelity data, AI allows for the capturing of potentially complex relationships between turbulence mean-flow characteristics (features) and modeling terms (predictions)

In the last years AI has been widely used in RANS models, employing a variety of methods for addressing a wide range of problems (Milano and Koumoutsakos [2002], Lecun et al. [2015], Ling and Templeton [2015], Ling et al. [2016a]). One such method that has gained attention for its flexibility and precision is deep learning (DL), which involves transforming input features through multiple layers of nonlinear interaction (Ling et al. [2016b]).

Turbulence, however, is a highly complex phenomenon that often proves challenging to accurately model using conventional AI techniques like deep learning (DL). One of the primary reasons for this complexity lies in the non-local effects of turbulence. The Reynolds stresses or turbulence stresses not only depend on the flow characteristics at the specific location where they are calculated but also on the flow characteristics in the surrounding regions. This interdependency poses a significant bottleneck in turbulence modeling. To address these non-linear problems more effectively, recurrent neural networks (RNN) are better suited due to their ability to capture spatial or temporal dependencies.

In particular, Long Short-Term Memory (LSTM) recurrent neural network is currently regarded as one of the most interesting types of neural networks, with potential for effectively capturing the non-locality of turbulence. LSTMs have found widespread applications in various fields, including language modeling, sentiment analysis, machine translation, speech recognition, and time series forecasting. In engineering, LSTMs are particularly useful for predicting trends and patterns in time series data, such as stock prices, weather patterns, electricity demand, anomaly detection in sensor data, industrial machinery health monitoring, and equipment failure prediction, among others (Hochritter and Schmidhuber [1997], Sutskever et al. [2014]). LSTMs excel in tasks where data has a sequential nature and long-term dependencies need to be captured, making them a promising approach for turbulence modeling.

In this study, an application of LSTM is performed to predict Reynolds stresses from data generated by Direct Numerical Simulation (DNS). The following section discusses aspects related to the Reynolds stress prediction using RNN; section 3 presents and discusses some of the LSTM models tested in the study; section 4 gives some numerical details of the RANS simulations; sec-

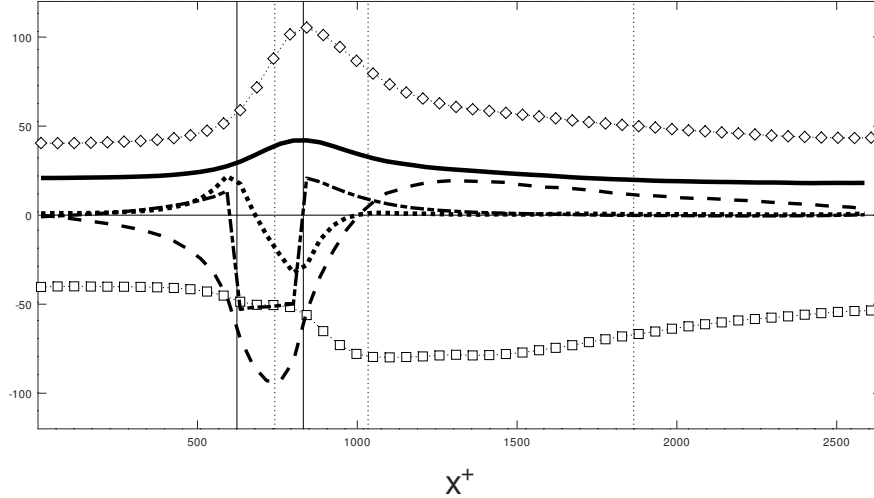


Figure 1: Mean flow and Reynolds stress dimensionless longitudinal profiles from DNS data for a channel flow with  $Re_\tau = 300$ , perturbed with an adverse pressure gradient at a narrow region of wide  $W^+ = 220$  at the buffer region. Vertical solid lines are the perturbation region limits, and the 3 vertical broken-lines, show middle,  $W^+$  and  $5W^+$  distance from perturbation region. Solid line,  $\partial U^+/\partial y^+$ ; - . - .  $-\partial P^+/\partial y^+$ ; - - -,  $20 \times \partial U^+/\partial x^+$ ; . . . .,  $20 \times \partial V^+/\partial x^+$ ;  $\square \cdot \square \cdot \square$ ,  $50 \times \langle uv \rangle^+$ ;  $\diamond \cdot \diamond \cdot \diamond$   $10 \times \langle vu \rangle^+$ .

tion 5 discusses and shows the results of the neural network fitting and propagation of predictions through RANS simulations, and finally section 6 lists some conclusions.

## 2 Reynolds stress prediction with LSTM RNN

Name	$R_\tau$	Perturbation	Parameter	Purpose
Developed	300			train. test.
BRE3006	300	blowing	$v^+ = 0.6$	train. test.
SRE3006	300	suction	$v^+ = 0.6$	train. test.
APGRE30025	300	adv. p. grad. step	$\partial P^+/\partial x^+ = +0.25$	train. test.
FPGRE30025	300	fav. p. grad. step	$\partial P^+/\partial x^+ = -0.25$	train. test.
BRE3004	300	blowing	$v^+ = 0.4$	val.
SRE3004	300	suction	$v^+ = 0.4$	val.
APG100045	600	adv. p. grad. step	$\partial P^+/\partial x^+ = +0.40$	val.
FPG100045	600	fab. p. grad. step	$\partial P^+/\partial x^+ = -0.40$	val.
Developed	1000			val.

Table 1: Data set for training, testing or validation.  $v^+$  is the dimensionless wall-normal velocity in the slot at the wall;  $\partial P^+/\partial x^+$  is the pressure gradient step in the perturbation region.

One of the most challenging aspects of turbulence is its non-local nature. Let's consider a scenario where we have a statistically stationary turbulent flow (the mean flow characteristics remain constant with time). When this flow is disturbed by an immersed body, for example, the primary effect is on the pressure field, mainly upstream and around the body. These pressure field changes

subsequently influence the mean velocity field around the object, resulting in an increase in turbulence primarily downstream of the body. In other words, the modifications in mean pressure and velocity, and turbulence fields, occur in different regions of the flow, emphasizing the non-local characteristics of turbulent flows.

Figure 1 shows the longitudinal profiles of mean flow and Reynolds stress in a channel flow perturbed by an adverse pressure gradient in a narrow region near the wall. This figure reveals that the maximum values of the shear Reynolds stress  $\langle uv \rangle$  occurs downstream of the perturbation region, which is clearly downstream where the maximum changes in the mean pressure and velocity are observed.

In the context of RANS turbulence models, such as the  $\kappa - \epsilon$  model (Pope [2000]), the inclusion of non-local effects is achieved through the convection and diffusion of kinetic energy ( $\kappa$ ) and turbulence dissipation ( $\epsilon$ ). However, incorporating these non-local effects becomes more challenging when using a regression model in deep learning (DL). In this case, it is more appropriate to utilize a recurrent neural network such as LSTM.

Another aspect of an NN model for Reynolds stress is its universality. The question arises regarding the level of universality and complexity the model should possess, or conversely, how specialized and simple it can be. Developing a universal model with an NN would necessitate a large number of adjustable parameters to capture all possible flow characteristics. Furthermore, fine-tuning an NN with a high parameter count is exceedingly challenging, and integrating a neural network with a large number of parameters into a computational fluid dynamics (CFD) software presents a significant obstacle due to the substantial computational demands it entails.

Consequently, this study aims to utilize an RNN with a reduced parameter count for rapid prediction in a RANS simulation. To achieve this, the LSTM neural network was trained, tested, and validated, using data generated from Direct Numerical Simulations (DNS) of fully developed or perturbed (developing) turbulent flows. All the flows considered in this study are statistically 2D channel flows, comprising the following scenarios: a) developed flows; b) flows perturbed with wall injection; c) flows perturbed with wall suction; d) flows perturbed with an adverse pressure gradient in a localized region; and e) flows perturbed with a favorable pressure gradient in a localized region. Each perturbed flow initially represents a developed flow, with a small region of width  $W^+ = 220$  being perturbed. To generate boundary conditions for a perturbed flow, two parallel DNS simulations were conducted, with the first simulation employing periodic boundary conditions. For more detailed information, please refer to the bibliography for additional insights (Pasinato [2012]). Table 1 provides a comprehensive list of the flows utilized in the study, accompanied by pertinent details such as perturbation parameters and their respective purposes.

Given that the turbulent flows studied are statistically stationary, the neural network is trained using space-sequences instead of time-sequences. Each space-sequence consists of 64 consecutive values along the longitudinal direction, with an approximate dimensionless distance of  $X^+ \simeq 41$  between each value. Consequently, the complete sequence covers a distance of approximately  $X^+ \simeq 2620$ , representing the entire physical domain. In other words, if for a DNS with  $R_\tau = 300$  a numerical grid with  $N = 254$  nodes is used in the longitudinal direction, for each spatial sequence  $N/4$  nodes of the DNS solution are employed at a fixed  $y^+$  distance from the wall.

To ensure a diverse representation during training, the full sequences are randomly shuffled. Additionally, the values are normalized between 0 and 1, using the global maximum and minimum values of the data set. This normalization process enables consistent scaling across different variables. Finally, the entire data set is exclusively divided into training and testing data, with the testing data comprising 20% of the complete data set.

### 3 LSTM models

Name	Parameters	Learning rate	Features	Predictions
L110DL	531	0.025-0.001	$S_{11}^+; S_{12}^+$	$\langle uv \rangle^+$
L15L25DL	386	0.025-0.001	$S_{11}^+; S_{12}^+$	$\langle uv \rangle^+$
L15DL-Y	186	0.025-0.001	$S_{11}^+; S_{12}^+; Y$	$\langle uv \rangle^+$
L110DL-Y	571	0.025-0.001	$S_{11}^+; S_{12}^+; Y$	$\langle uv \rangle^+$

Table 2: LSTM tested models.

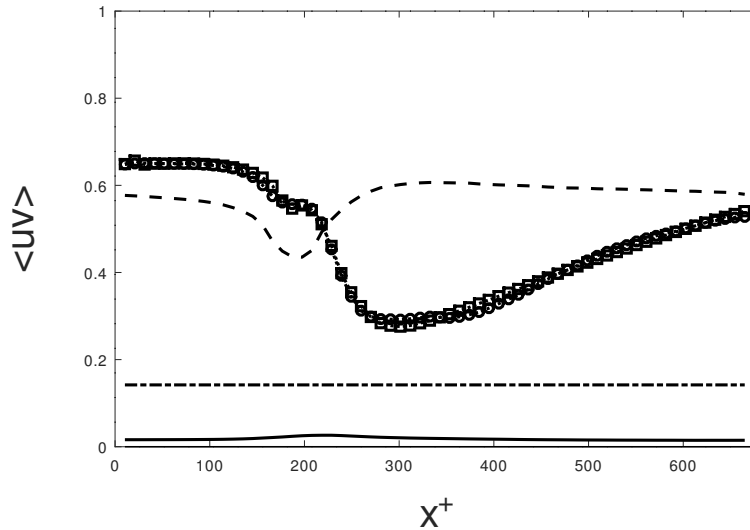


Figure 2: Prediction of  $\langle uv \rangle^+$  with the LSTM model L110DL-Y. Solid line,  $S_{12}^+$ ; ---,  $S_{11}^+$ ; - . - . -,  $y/\delta$ ;  $\square \cdot \square \cdot \square$ , Prediction;  $\circ \cdot \circ \cdot \circ$ , DNS data. The data set was normalized in the 0-1 range with the global maximum and minimum.

All LSTM models were implemented in two different numerical codes: one developed in-house using modern Fortran, and the other implemented in Python using the Keras-TensorFlow libraries (Abadi et al. [2015]). The purpose of the Fortran code was to gain insight into the forward and backward algorithms of LSTM and compare them with the Keras version (Chen [2018]).

The LSTM, like other deep learning models, has three hyper-parameters: a) the number of stacked layers (or stacked LSTM cells), b) the number of memory units in each LSTM layer, and c) the learning rate. In this study, these hyper-parameters were selected through trial and error.

It is worth mentioning that the TensorFlow libraries offer a wide range of optimization methods, including dynamic learning-rate techniques that speed up convergence. However, both the Fortran and Keras codes faced challenges when optimizing models with many stacked layers (5 or more layers) and numerous memory units. To simplify the models and reduce the number of parameters, a maximum of 3 stacked LSTM layers with a maximum of 10 memory units were used for all tested models. Finally the best predicted solution were from models with 1 LSTM cell and 10 memory units for the data set used.

Table 2 presents some of the LSTM models tested in this study. The name *L15L25DL* indicates an LSTM with 2 stacked layers, each having 5 memory units, and a dense output layer. The

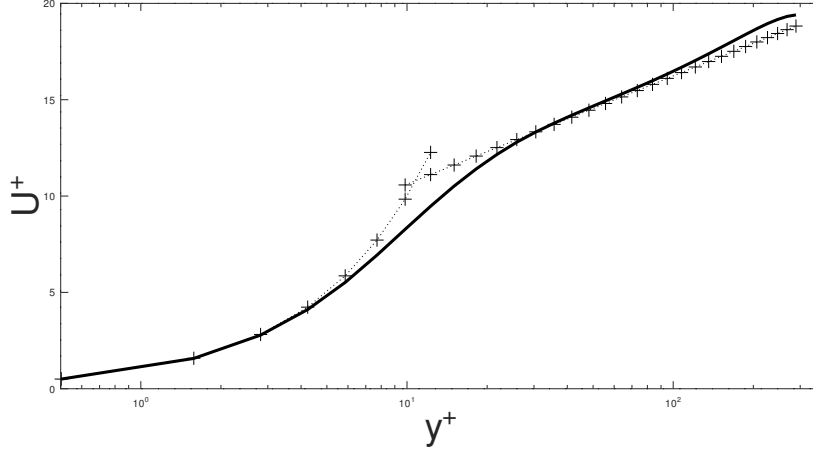


Figure 3: Mean velocity for a developed channel flow with  $Re_\tau = 300$  with  $\langle uv \rangle^+$  predicted from the LSTM model L110DL-Y. Solid line,  $U^+$ ; + · + · +, Logarithmic profile  $1/0.41 \ln(y^+) + 5.5$ .

components  $S_{11}^+$  and  $S_{12}^+$  represent the dimensionless mean rate-of-strain-tensor  $S_{ij}$ , which are calculated as  $S_{ij}^+ = 1/2(\partial U_i^+/\partial x_j^+ + \partial U_j^+/\partial x_i^+)$ . Additionally,  $Y$  denotes the dimensionless wall distance ( $y/\delta$ ). It is important to note that the axes in  $S_{ij}$  are non-dimensionalized differently from the distance to the wall  $Y$ .

Although the primary objective of this study was to predict the shear Reynolds stress  $\langle uv \rangle$ , some of the models were developed to predict the normal Reynolds stress  $\langle uu \rangle$ , as an initial step, followed by an LSTM model to predict  $\langle uv \rangle$  based on the predicted  $\langle uu \rangle$ . In all of these cases, the optimization of the LSTM models for  $\langle uu \rangle$  yielded superior and faster results compared to the LSTM models for  $\langle uv \rangle$ .

The previous architecture of one RNN to predict  $\langle uu \rangle$  and a second RNN to predict  $\langle uv \rangle$  is based on the non-linearity of turbulence. In the context of channel turbulent flows, it is well-established that turbulence acquires energy from the mean flow first through  $\langle uu \rangle$ . Subsequently, the instantaneous pressure field transfers a portion of this energy to the  $\langle vv \rangle$  and  $\langle ww \rangle$  components (Tennekes and Lumley [1972]). As consequence as depicted in Fig. 1, the modification of  $\langle uu \rangle$  occurs promptly after the mean velocity and pressure field are perturbed, while the alteration of  $\langle uv \rangle$  experiences a certain delay. No results are presented here of the LSTM model of  $\langle uv \rangle$  based on a previous prediction of  $\langle uu \rangle$ .

## 4 Numerical details of the RANS simulations

The RANS simulations with the propagation of the LSTM predictions and the  $\kappa - \epsilon$  model were computed with a physical domain of  $3\pi\delta \times 2\delta \times 4/3\pi\delta$ , and a numerical grid of  $64 \times 64 \times 64$  ( $\Delta x^+ = 44$ ,  $\Delta z^+ = 19.6$ ,  $\Delta y_{max}^+ = 26.4$ , and  $\Delta y_{min}^+ = 1$ ), and the time step  $0.15\nu/u_\tau^2$ . In the wall-normal direction a non-uniform mesh distributed with the hyperbolic tangent function is used and the expansion ratio is adjusted to ensure that the  $y^+$  of the first cell center is equal to 1. Furthermore, a van Driest function near the wall is used with the  $\kappa - \epsilon$  model. Considering the low Reynolds number flows employed in this study, it is believed that the wall modeling approach adopted is adequate.

The RANS simulation of perturbed flow follows a similar approach to DNS. Initially, a fully

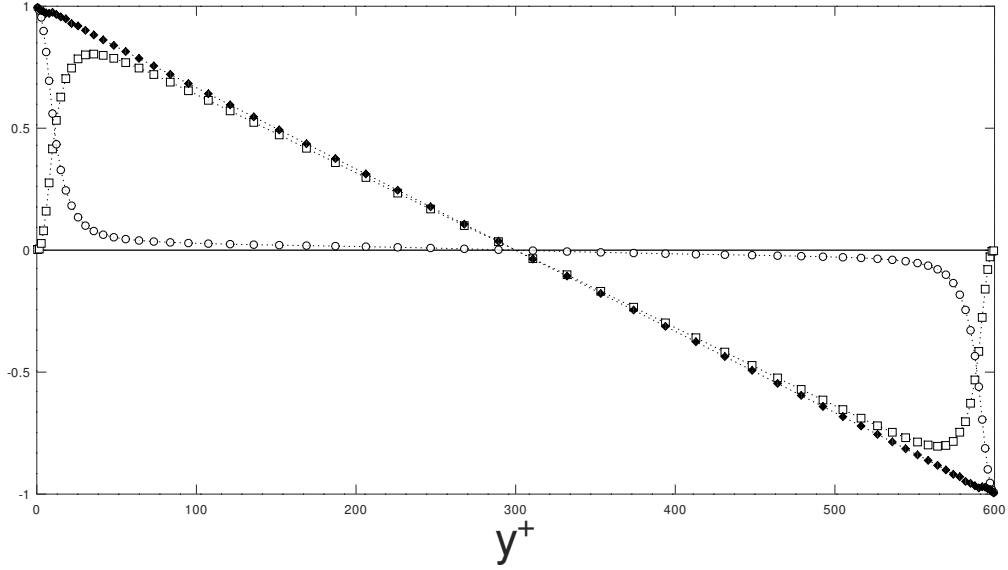


Figure 4: Shear stresses for a developed channel flow with  $Re_\tau = 300$  with  $\langle uv \rangle^+$  predicted with the LSTM model L110DL-Y. Filled diamonds, total stresses;  $\square \cdot \square \cdot \square$ ,  $\langle uv \rangle^+$ ;  $\circ \cdot \circ \cdot \circ$ , molecular stress  $dU^+/dy^+$ .

developed flow is considered, and a small region of width  $W_+=220$  is perturbed. To generate boundary conditions for the perturbed flow, a second simulation is conducted in parallel with periodic boundary conditions, representing the fully developed flow. In other words, at every time-step, the input boundary condition for the perturbed flow is extracted from the middle of the computational domain of the fully developed flow.

## 5 Results and Discussion

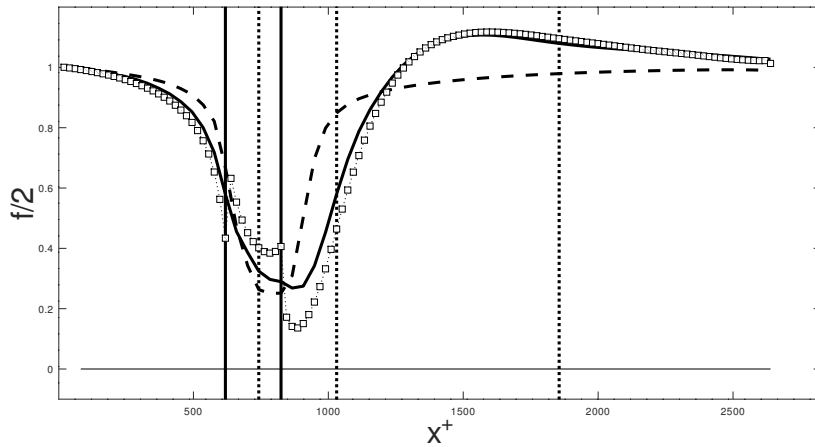


Figure 5: Comparison of half of the skin-friction for a channel flow with  $Re_\tau = 300$  perturbed with blowing with an injection dimensionless velocity 0.40 from a narrow slot at the wall, with  $\langle uv \rangle^+$  predicted with the LSTM L110DL-Y model. Solid line, LSTM;  $- - -$ ,  $\kappa - \epsilon$  model;  $\square \cdot \square \cdot \square$ , DNS.

In this section, we present the results of the LSTM predictions and their integration with a

CFD code for propagation. The term "propagation" refers to the utilization of the LSTM RNN as a substitute for a RANS turbulence model. At each time-step, sequences are formed and the LSTM model is employed to calculate the Reynolds stress  $\langle uv \rangle$  at every node of the grid. While we provide some comparisons between the LSTM prediction and results obtained from the  $\kappa - \epsilon$  model (which computes all shear and normal Reynolds stresses), the RANS simulations with LSTM predictions only consider the shear Reynolds stress  $\langle uv \rangle$ . The remaining Reynolds stresses were taken equal to zero.

As mentioned earlier, the purpose of using the LSTM RNN in this study is not to capture the universal behavior of turbulence, but rather to predict statistical stationary 2D turbulent flows specifically for channel flow. The LSTM model serves as a proof of concept for predicting Reynolds stresses. Consequently, the turbulent flows utilized for validating the LSTM model share certain similarities with the flows employed for model adjustment and testing.

For instance, all the turbulent flows used for model adjustment, testing, and validation pertain to channel flows. These flows encompass developed or perturbed developing flows, characterized by low or medium friction Reynolds numbers  $Re_\tau$  (300-1000). It is worth noting that the mean velocity and normal Reynolds stresses, along with other statistical measures, exhibit low Reynolds number effects in these flows. The developing flows represent turbulent flows that have been perturbed from the wall or in small regions in the buffer region.

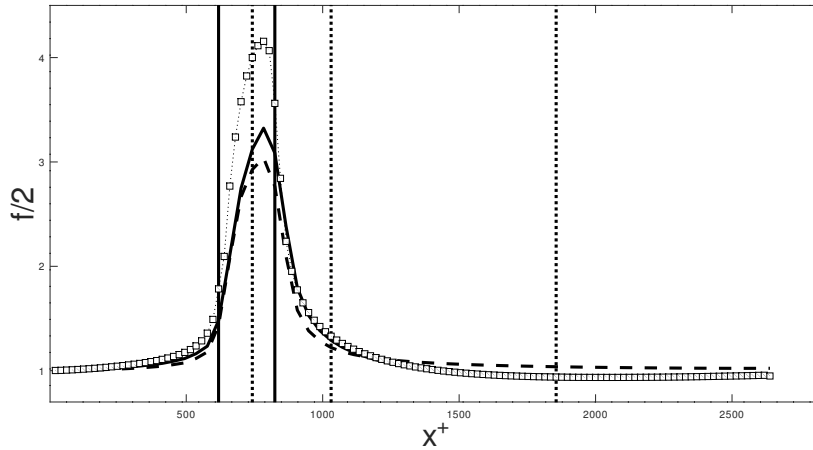


Figure 6: Comparison of half of the skin-friction for a channel flow with  $Re_\tau = 300$  perturbed with suction from a narrow slot at the wall, with  $\langle uv \rangle^+$  predicted with the LSTM L110DL-Y model. Solid line, LSTM;  $---$ ,  $\kappa - \epsilon$  model;  $\square \cdot \square \cdot \square$ , DNS.

*Prediction of the shear Reynolds stress without propagation:* Figure 2 illustrates the LSTM-based prediction of the shear Reynolds stress  $\langle uv \rangle^+$  utilizing  $S_{11}^+$ ,  $S_{12}^+$ , and  $Y(= y/\delta)$  as input parameters, with L110DL-Y model. The LSTM model employed for this prediction follows a sequence-by-sequence (seqxseq) architecture (Sutskever et al. [2014]). To ensure consistent scaling, all data points have been normalized within the range of 0-1, utilizing the global minimum and maximum values across the entire dataset. These normalized values are subsequently transformed back to their original, real-world scale using the same minimum and maximum values.

*Propagation of predicted shear Reynolds stress in developed flow:* In fully developed turbulent flows, the momentum equation (2) in the longitudinal direction can be expressed in dimensionless form using the characteristic velocity scale  $u_\tau$  and boundary layer thickness  $\delta$ , as mentioned earlier.



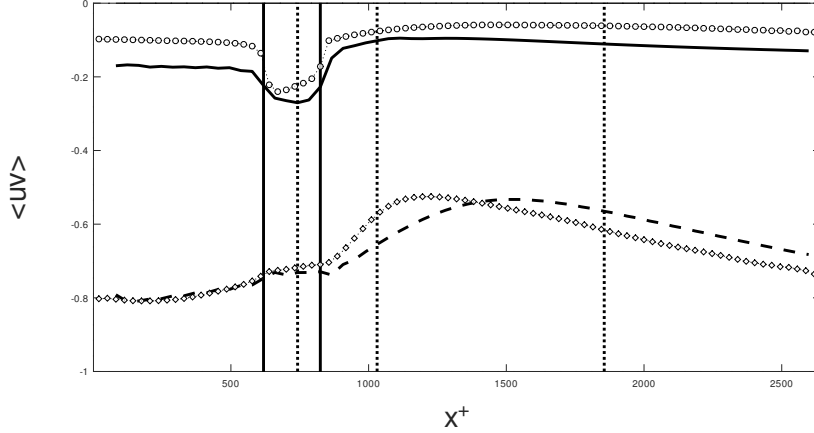


Figure 7: Comparison of the shear Reynolds stress for a channel flow with  $Re_\tau = 300$  perturbed with suction from a narrow slot at the wall, with  $\langle uv \rangle^+$  predicted from the L110DL-Y model.  $y^+ = 5$ , solid line, LSTM;  $\circ \cdot \circ \cdot \circ$  DNS;  $y^+ = 30$ , - - -, LSTM;  $\diamond \cdot \diamond \cdot \diamond$ , DNS.

It takes the following form:

$$\frac{dU^+}{dy^+} = \langle uv \rangle^+ + \left(1 - \frac{y^+}{R_\tau}\right) \quad (3)$$

where the pressure gradient has been substituted with the wall shear stress (Tennekes and Lumley [1972]). Equation (3) illustrates the equilibrium between the Reynolds shear stress and the wall-normal gradient of the longitudinal mean velocity for a fully developed turbulent flow. This equilibrium is depicted in the plots of  $U^+$ ,  $\langle uv \rangle^+$ , and  $dU^+/dy^+$  as functions of the dimensionless distance to the wall,  $y^+$ , in Figs. 3 and 4. Specifically, the agreement of the  $U^+$  profile with the logarithmic law of the wall in the logarithmic sub-region, shown in Fig. 3, indicates that the predicted value of  $\langle uv \rangle^+$  is accurate.

Thus, as observed in these figures, the mean velocity exhibits a logarithmic sub-region with appropriate values for the given Reynolds number, indicating the characteristic velocity profile of a developed turbulent flow. Furthermore, the shear stresses, including both molecular and turbulent components, demonstrate a state of perfect equilibrium under developed flow conditions. This implies that the LSTM predictions successfully capture the essential features of developed turbulent flows.

In order to evaluate the stability of the results obtained from the LSTM model, a series of tests were conducted using flows with initial conditions significantly distant from a fully developed state. The objective of these tests was to assess the capability of the LSTM model to converge towards a stable solution.

*Propagation of predicted shear Reynolds stress in developing flows:* In this section the results of the LSTM model L110DL-Y propagated in developing turbulent channel flow are presented. The first case is a blowing case in a channel with a dimensionless injection velocity of 0.40 (the set of data for training included an injection case with a dimensionless injection velocity of 0.60). The results of the propagated LSTM predictions are shown in comparison with  $\kappa - \epsilon$  model and data from DNS, Figs. 5 to 7.

Figures 5 and 6 clearly demonstrate the LSTM model's superior performance in computing the skin friction when compared to the traditional  $\kappa - \epsilon$  model. Additionally, Figure 7 illustrates that

the propagated shear Reynolds stress follows the general trend observed in the DNS data.

A RANS prediction depends on various factors, such as the numerical grid, software precision, and, of course, the RANS model itself. In this study, all these aspects were reasonably implemented. Based on the presented comparisons between the LSTM RNN and the  $\kappa - \epsilon$  model predictions, it can be concluded that LSTM-RANS exhibits superior performance. However, it is essential to note that the LSTM-RANS simulations with the L110DL-Y model used here required approximately 50% more time for computation than  $\kappa - \epsilon$  simulations.

Regarding the time-processing aspect of LSTM-RANS, it is worth mentioning that a more comprehensive study should be conducted. This broader investigation should encompass the use of different RANS models and LSTM networks with varying numbers of parameters to draw more definitive conclusions.

In summary, the study demonstrates that LSTM-RANS outperforms the traditional  $\kappa - \epsilon$  model, but further research is needed to explore its efficiency and effectiveness fully.

## 6 Conclusions

In this study, we introduce the application of an artificial Recurrent Neural Network (RNN) known as LSTM as a promising alternative to a turbulent RANS model. The primary objective was to utilize the LSTM model for predicting the shear Reynolds stress in both developed and developing turbulent channel flows, and subsequently propagate this prediction.

To assess its performance, we conduct a comparative analysis, where we compare the LSTM results, propagated through CFD simulations, with the outcomes from the traditional  $\kappa - \epsilon$  model and data obtained from DNS. Remarkably, the LSTM approach demonstrates a strong performance in these analyses, showing its potential as an effective technique for modeling the shear Reynolds stress in turbulent flows.

It is essential to note that this study serves as a proof of concept, and the validation process utilizes 2D statistical turbulent flows as the training and test data sets. Despite this limitation, the results presented here indicate the LSTM RNN's efficacy in modeling the shear Reynolds stresses accurately in turbulent flows.

Overall, the findings from this study open up exciting possibilities for further exploring the capabilities of LSTM models as alternatives to conventional RANS models in the context of turbulence prediction and modeling.

## References

- S. Pope. *Turbulent Flow*. University Press, Cambridge, Cambridge, UK, 1st. edition, 2000.
- M. Milano and P. Koumoutsakos. Neural network modeling for near wall turbulent flow. *J. Comp. Physics*, pages 1–12, 2002. doi: 10.1006/jcph.2002.7146.
- Y. Lecun, Y. Bengio, and G. Hinton. Deep learning. *Nature*, 521, 2015. doi: 10.1038/nature14539.
- J. Ling and J. Templeton. Evaluation of machine learning algorithms for prediction of regions of high Reynolds-averaged Navier-Stokes uncertainty. *Phys. Fluids*, 27:99, 2015.

- J. Ling, Jones R., and J. Templeton. Machine learning strategies for systems with invariance properties. *J. Comput. Phys*, pages 22–35, 2016a.
- J. Ling, Kurzawski A., and Templeton J. D. Reynolds averaged turbulence modelling using deep neural networks with embedded invariance. *J. Fluid Mechanics*, 807:155–166, 2016b.
- S. Hochritter and J. Schmidhuber. Long short term memory. *Neural Computation*, 9:1–32, 1997.
- I. Sutskever, Vinyals O., and Quoc V. Le. Sequence to sequence learning with neural networks. *arXiv*, pages 1–9, 2014. doi: org/10.48550/arXiv.1409.3215.
- H. D. Pasinato. Dissimilarity of turbulent fluxes of momentum and heat in perturbed turbulent flows. *J. Heat Transfer-ASME*, 135:1–12, 2012.
- Martín Abadi, Ashish Agarwal, Paul Barham, Eugene Brevdo, Zhifeng Chen, Craig Citro, Greg S. Corrado, Andy Davis, Jeffrey Dean, Matthieu Devin, Sanjay Ghemawat, Ian Goodfellow, Andrew Harp, Geoffrey Irving, Michael Isard, Yangqing Jia, Rafal Jozefowicz, Lukasz Kaiser, Manjunath Kudlur, Josh Levenberg, Dandelion Mané, Rajat Monga, Sherry Moore, Derek Murray, Chris Olah, Mike Schuster, Jonathon Shlens, Benoit Steiner, Ilya Sutskever, Kunal Talwar, Paul Tucker, Vincent Vanhoucke, Vijay Vasudevan, Fernanda Viégas, Oriol Vinyals, Pete Warden, Martin Wattenberg, Martin Wicke, Yuan Yu, and Xiaoqiang Zheng. TensorFlow: Large-scale machine learning on heterogeneous systems, 2015. URL <https://www.tensorflow.org/>. Software available from tensorflow.org.
- G. Chen. A gentle tutorial of recurrent neural network with error backpropagation. pages 1–10, 2018.
- H. Tennekes and J. L. Lumley. *A First Course in Turbulence*. MIT Press, Cambridge USA, 1972.